Supporting Information

Discovery, Optimization, and Evaluation of Quinazolinone Derivatives with Novel Linkers as Orally Efficacious Phosphoinositide-3-Kinase delta Inhibitors for the Treatment of Inflammatory Diseases

Kongjun Liu[a,§], Dan Li[a,§], Wei Zheng[a,§], Mingsong Shi[a,§], Yong Chen[a], Minghai Tang[a], Tao Yang[a], Min Zhao[a], Dexin Deng[a], Chufeng Zhang[a], Jiang Liu[a], Xue Yuan[a], Zhuang Yang[a,*], and Lijuan Chen[a,*]

[a] Laboratory of Natural and targeted small molecule drugs, State Key Laboratory of Biotherapy and Cancer Center, National Clinical Research Center for Geriatrics, West China Hospital, Sichuan University and Collaborative Innovation Center of Biotherapy, Chengdu, 610041, China

[§] These authors contributed equally and should be considered as co-first authors.

[*] Lijuan Chen. Tel: +86-28-85164063; E-mail address: chenlijuan125@163.com.

[*] Zhuang Yang. Tel: +86-28-85164063; E-mail address: young9008@126.com.

Table of Contents for Support Information

Table S1. Kinome Wide Selectivity Profiling of Compound **50**

Kinase	Kinase family	Percent control (%) at 10 μM
AAK1(h)	MISC	91
Abl(h)	TK	113
ACK1(h)	TK	107
ACTR2(h)	TKL	83
ALK(h)	TK	148
Arg(h)	TK	134
AMPKα1(h)	CAMK	92
A-Raf(h)	TKL	76
ASK1(h)	STE	107
Aurora-A(h)	MISC	85
Axl(h)	TK	111
Blk(h)	TK	85
BMPR2(h)	TKL	99
Bmx(h)	TK	128
BRK(h)	TK	95
BrSK1(h)	CAMK	118
BTK(h)	TK	97
B-Raf(h)	TKL	94
CaMKI(h)	CAMK	108
CDK1/cyclinB(h)	CMGC	124
CDK2/cyclinA(h)	CMGC	86
CDK6/cyclinD3(h)	CMGC	103
CDK7/cyclinH/MAT1(h)	CMGC	117
CDK9/cyclin T1(h)	CMGC	104
CHK1(h)	CAMK	102
CK1γ1(h)	CK1	91
CK2α2(h)	CMGC	94
CLIK1(h)	MISC	112
cKit(V654A)(h)	TK	79
c-RAF(h)	TKL	91
DAPK1(h)	CAMK	102
DCAMKL2(h)	CAMK	79
DDR1(h)	TK	84
DMPK(h)	AGC	100
DRAK1(h)	CAMK	128
DYRK1A(h)	CMGC	112
eEF-2K(h)	MISC	98
EGFR(h)	TK	116

EphB4(h)	TK	90
FAK(h)	TK	112
Fer(h)	TK	89
Fes(h)	TK	95
FGFR1(h)	TK	113
Fgr(h)	TK	108
Flt3(h)	TK	80
Fms(h)	TK	94
Fyn(h)	TK	118
GCK(h)	STE	79
GCN2(h)	MISC	114
GRK1(h)	AGC	77
GSK3β(h)	CMGC	105
HIPK1(h)	CMGC	89
HRI(h)	MISC	88
ICK(h)	CMGC	79
IGF-1R(h)	TK	135
IKKα(h)	MISC	120
IR(h)	TK	106
IRAK4(h)	TKL	132
Itk(h)	TK	106
JAK1(h)	TK	97
JAK2(h)	TK	102
JNK1α1(h)	CMGC	95
KDR(h)	TK	96
Lck(h)	TK	79
LIMK1(h)	TKL	79
LOK(h)	STE	109
Lyn(h)	TK	95
LRRK2(h)	TKL	90
LTK(h)	TK	93
MAPK1(h)	CMGC	93
MAP4K3(h)	STE	75
MAPKAP-K2(h)	CAMK	103
MEK1(h)	STE	104
MARK1(h)	CAMK	76
MEKK2(h)	STE	90
Mer(h)	TK	100
MINK(h)	STE	110
MKK6(h)	STE	79
MLK1(h)	TKL	73

Mnk2(h)	CAMK	90
MRCKα(h)	AGC	94
MSK1(h)	AGC	129
MSK2(h)	AGC	101
MST1(h)	STE	127
mTOR(h)	Lipid/Atypical	65
mTOR/FKBP12(h)	Lipid/Atypical	74
MuSK(h)	TK	86
MYLK2(h)	CAMK	107
MYO3B(h)	STE	79
NDR2(h)	AGC	103
NEK2(h)	MISC	119
NIM1(h)	CAMK	123
NLK(h)	CMGC	90
p70S6K(h)	AGC	75
PAK2(h)	STE	97
PAR-1Bα(h)	CAMK	73
PASK(h)	CAMK	98
PDGFRβ(h)	TK	102
PDK1(h)	AGC	104
PhKγ1(h)	CAMK	89
Pim-1(h)	CAMK	108
PKA(h)	AGC	100
PKBα(h)	AGC	114
PKCα(h)	AGC	113
PKCθ(h)	AGC	123
PKD2(h)	CAMK	100
PKG1α(h)	AGC	81
Plk3(h)	MISC	100
PRAK(h)	CAMK	115
PRK1(h)	AGC	85
PRP4(h)	CMGC	105
Ret(h)	TK	103
RIPK1(h)	TKL	98
ROCK-I(h)	AGC	101
Ron(h)	TK	74
Ros(h)	TK	84
Rse(h)	TK	114
Rsk1(h)	AGC	143
Rsk2(h)	AGC	110
SAPK2a(h)	CMGC	97

SBK1(h)	MISC	124
SGK(h)	AGC	103
SIK(h)	CAMK	98
SNRK(h)	CAMK	106
Src(1-530)(h)	TK	81
SRMS(h)	TK	92
SRPK1(h)	CMGC	117
STK16(h)	MISC	82
Syk(h)	TK	72
TAK1(h)	TKL	124
TBK1(h)	MISC	97
Tec(h) activated	TK	78
TGFBR1(h)	TKL	88
Tie2 (h)	TK	91
TLK1(h)	MISK	90
TNIK(h)	STE	76
TrkA(h)	TK	86
TSSK1(h)	CAMK	73
TTBK1(h)	CK1	91
TTK(h)	MISC	104
Txk(h)	TK	90
TYK2(h)	TK	83
ULK1(h)	MISC	99
VRK1(h)	CK1	96
Wee1(h)	MISC	90
WNK1(h)	MISC	100
Yes(h)	TK	103
ZAK(h)	TKL	93
ZAP-70(h)	TK	109
ZIPK(h)	CAMK	108
ATM(h)	Lipid/Atypical	120
ATR/ATRIP(h)	Lipid/Atypical	95
PI3 Kinase (p110δ/p85α)(h)	Lipid/Atypical	-10
PI3 Kinase (p110α/p85α)(h)	Lipid/Atypical	45
PI3 Kinase (p110α(E542K)/p85α)(h)	Lipid/Atypical	31
PI3 Kinase (p110α(H1047R)/p85α)(h)	Lipid/Atypical	14
PI3 Kinase (p110α(E545K)/p85α)(h)	Lipid/Atypical	25
PI3 Kinase (p110α/p65α)(h)	Lipid/Atypical	20
PI3KC2α(h)	Lipid/Atypical	91
PI3KC2γ(h)	Lipid/Atypical	53
PIP4K2α(h)	Lipid/Atypical	101

PIP5K1α(h)	Lipid/Atypical	96
PIP5K1γ(h)	Lipid/Atypical	87

Table S2. Predicted results of compound **43** from the CYP3A4 model in SMARTCyp[a]

3A4 Ranking	Atom	3A4 Score	Energy	2DSASA	Span2end	Relative Span	Similarity
1	C.23	34.0	41.1	31.0	3	0.7	0.7
2	C.11	36.4	41.1	7.3	5	0.5	0.3
3	N.16	44.1	54.1	50.2	0	1.0	0.7
4	C.21	48.3	57.9	39.6	0	1.0	1.0
5	N.12	58.8	63.9	1.3	4	0.6	0.3
6	C.30	59.1	68.2	27.4	0	1.0	1.0
7	N.17	66.9	75.6	17.8	0	1.0	0.3
8	N.14	68.6	75.6	10.5	2	0.8	0.3
9	C.24	68.7	75.9	35.1	3	0.7	0.7
10	C.28	69.5	77.2	27.6	2	0.8	1.0
11	C.25	69.6	75.9	29.5	4	0.6	0.3
12	N.26	70.3	75.6	6.1	4	0.6	0.3
13	C.29	72.3	80.8	31.6	1	0.9	1.0
14	C.7	76.9	86.3	36.2	0	1.0	1.0
15	C.6	77.7	86.3	33.5	1	0.9	1.0
16	C.5	78.6	86.3	27.6	2	0.8	1.0
17	N.20	83.9	92.1	22.1	1	0.9	0.7

[a] The atoms in the table are ranked by score, with the lowest score resulting in the lowest rank, and thus the highest probability of being a site of metabolism.

Table S3. Predicted results of compound **43** from the CYP2D6 model in SMARTCyp[a]

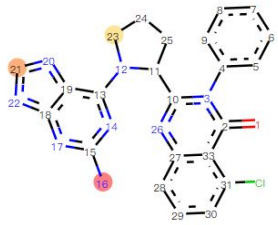

2D6 Ranking	Atom	2D6 Score	Energy	2DSASA	Span2end	N+dist	Similarity
1	N.16	52.1	54.1	50.2	0	0	0.7
2	C.21	56.3	57.9	39.6	0	0	1.0
3	C.23	60.0	41.1	31.0	3	0	0.7
4	C.30	67.1	68.2	27.4	0	0	1.0
5	C.11	67.7	41.1	7.3	5	0	0.3
6	N.17	74.9	75.6	17.8	0	0	0.3
7	C.7	84.9	86.3	36.2	0	0	1.0
8	C.29	86.2	80.8	31.6	1	0	1.0
9	N.14	88.6	75.6	10.5	2	0	0.3
10	C.28	89.5	77.2	27.6	2	0	1.0
11	N.12	90.7	63.9	1.3	4	0	0.3
12	C.6	91.7	86.3	33.5	1	0	1.0
13	C.24	94.6	75.9	35.1	3	0	0.7
14	N.20	97.9	92.1	22.1	1	0	0.7
15	C.5	98.6	86.3	27.6	2	0	1.0
16	C.25	101.6	75.9	29.5	4	0	0.3
17	N.26	102.2	75.6	6.1	4	0	0.3

[a] The atoms in the table are ranked by score, with the lowest score resulting in the lowest rank, and thus the highest probability of being a site of metabolism.

Table S4. Predicted results of compound **43** from the CYP2C9 model in SMARTCyp[a]

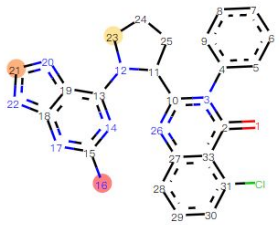

2C9 Ranking	Atom	2C9 Score	Energy	2DSASA	Span2end	COO-Dist	Similarity
1	N.16	52.1	54.1	50.2	0	0	0.7
2	C.21	56.3	57.9	39.6	0	0	1.0
3	C.23	57.6	41.1	31.0	3	0	0.7
4	C.11	64.5	41.1	7.3	5	0	0.3
5	C.30	67.1	68.2	27.4	0	0	1.0
6	N.17	74.9	75.6	17.8	0	0	0.3
7	C.7	84.9	86.3	36.2	0	0	1.0
8	C.29	85.4	80.8	31.6	1	0	1.0
9	N.14	87.0	75.6	10.5	2	0	0.3
10	N.12	87.5	63.9	1.3	4	0	0.3
11	C.28	87.9	77.2	27.6	2	0	1.0
12	C.6	90.9	86.3	33.5	1	0	1.0
13	C.24	92.2	75.9	35.1	3	0	0.7
14	C.5	97.0	86.3	27.6	2	0	1.0
15	N.20	97.1	92.1	22.1	1	0	0.7
16	C.25	98.4	75.9	29.5	4	0	0.3
17	N.26	99.0	75.6	6.1	4	0	0.3

[a] The atoms in the table are ranked by score, with the lowest score resulting in the lowest rank, and thus the highest probability of being a site of metabolism

Table S5. The effects of compound **50** and idelalisib on normal cells viability.

Cell line	Cell type	IC_{50} (mean ± SD) (uM)[a]		SI[b] (55, Normal cells/ Primary T cells)
		55	idelalisib	
H9C2	Rat myocardial cell line	＞20	＞20	＞965
L929	Mouse fibroblast cell line	＞20	＞20	＞965
HEK293	Human embryonic kidney epithelial cell line	16.08 ± 0.95	＞20	＞776
LO2	Human normal liver cell line	＞20	＞20	＞965

[a]IC_{50} values were obtained from three independent experiments. SI[b] = selectivity index, which represents the preliminary safety of compounds. Cells (H9C2, L929, HEK293, and LO2) were seeded in 96-well plates (1500/well) at individual density in 80 uL of culture medium for 24 h. After various concentrations of compound **50** and idelalisib treatment for 72 h, at 37℃ and 5% CO_2, 100 uL culture medium containing 10 uL CCK-8 solutions was added and incubated for 2 h at 37℃. The optical density was measured using Spectra MAX M5 microplate spectrophotometer (Molecular Devices) at 450 nm and the IC_{50} of each cell line was detected.

Table S6. Binding free energy (ΔG_{bind}^{cal}) for idelalisib/PI3Kδ complexes and decomposition to electrostatic interaction (E_{ele}), van der Walls interaction (E_{vdW}) and solvation free energies (E_{GB}). Energies are in kcal/mol.

Energy	Complex	Receptor	Ligand	Difference
E_{vdW}	-7626.74(43.21)	-7576.07(43.12)	-6.24(1.46)	-44.43(2.76)
E_{ele}	-64923.98(238.86)	-65035.18(238.65)	134.52(1.85)	-23.32(3.25)
E_{GB}	-10470.50(200.01)	-10480.76(200.00)	-23.26(0.63)	33.52(2.74)
E_{surf}	314.57(3.57)	316.26(3.56)	3.49(0.03)	-5.18(0.22)
G_{gas}	-10128.21(228.56)	-9853.30(228.27)	-207.17(4.94)	-67.74(3.92)
G_{solv}	-10155.93(198.60)	-10164.50(198.62)	-19.77(0.62)	28.34(2.68)
$E_{gas} + G_{sol}$	-20284.14(89.22)	-20017.80(89.07)	-226.94(4.94)	-39.40(2.64)

Table S7. Binding free energy (ΔG_{bind}^{cal}) for compound **50**/PI3Kδ complexes and decomposition to electrostatic interaction (E_{ele}), van der Walls interaction (E_{vdW}) and solvation free energies (E_{GB}). Energies are in kcal/mol.

Energy	Complex	Receptor	Ligand	Difference
E_{vdW}	-7679.32(43.84)	-7620.70(43.87)	-6.21(1.52)	-52.41(2.78)
E_{ele}	-65117.58(281.23)	-65146.89(281.35)	50.51(1.30)	-21.19(3.65)
E_{GB}	-10329.29(229.52)	-10341.91(229.58)	-20.14(0.53)	32.76(3.13)
E_{surf}	310.63(4.98)	312.80(4.98)	3.63(0.03)	-5.80(0.22)
G_{gas}	-10087.78(270.72)	-10001.42(270.93)	-12.76(5.25)	-73.60(4.28)
G_{solv}	-10018.66(226.22)	-10029.11(226.27)	-16.51(0.52)	26.95(3.06)
$E_{gas} + G_{sol}$	-20106.44(96.57)	-20030.53(96.37)	-29.26(5.26)	-46.65(2.83)

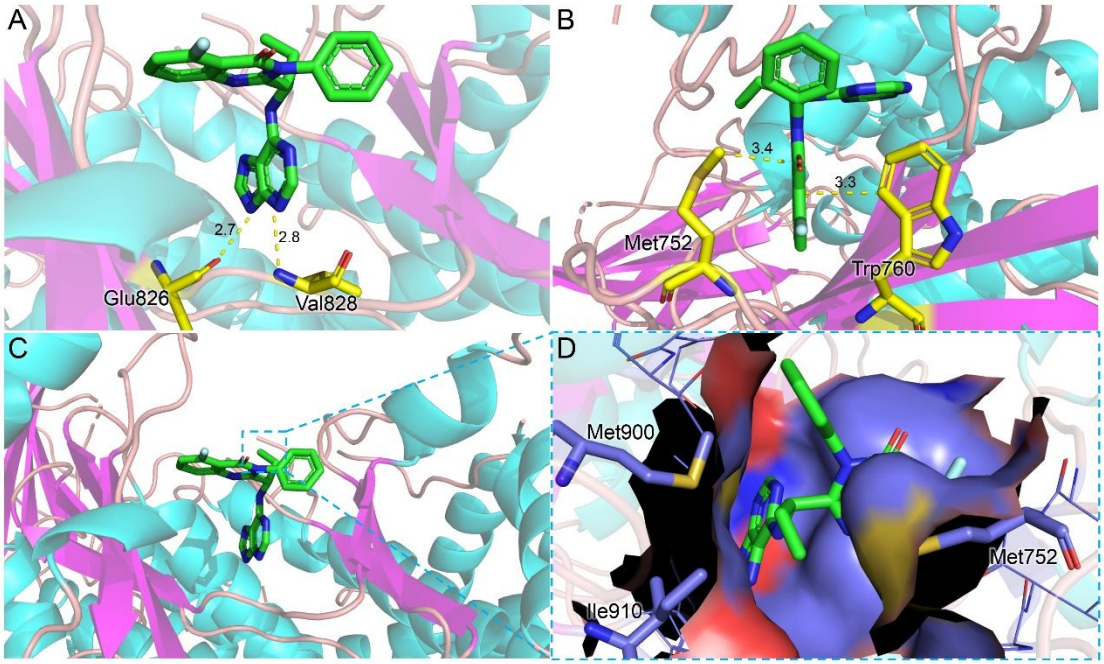

Figure S1. Cocrystal structure of **1** in PI3Kδ (PDB Code: 4XE0). (A) The purine moiety forms two hydrogen bonds with the backbones of Val-828 and Glu-826, respectively. (B) The quinazolinone motif makes a hydrophobic interaction with Met752 and Trp760. (C) Sticks figure of **1** bound to ATP binding site of the p110 catalytic subunits of PI3Kδ. (D) Surface figure of **1** in the binding pocket, the (S)-ethyl group is placed in a hydrophobic pocket formed by Met752, Met900, and Ile910.

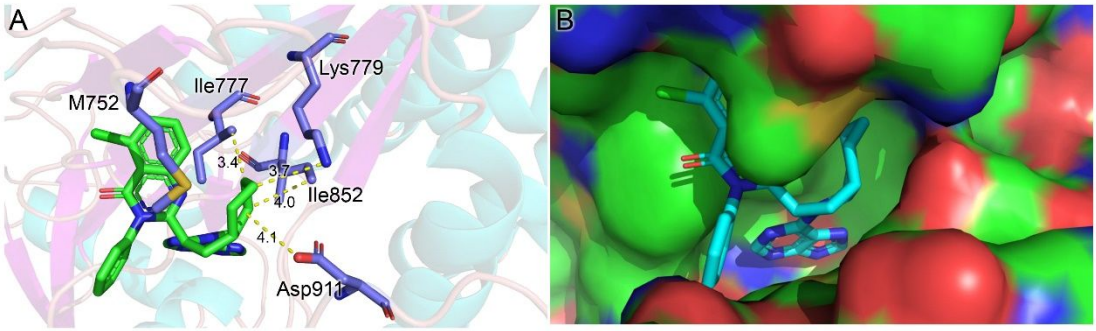

Figure S2. Docking model of compound **29** in PI3Kδ (PDB code:4XEO). (A) Sticks figure of **29** bound to PI3Kδ. (B) Surface figure of **29** bound to PI3Kδ. The small hydrophobic pockets formed by Ile777, Lys779, Ile825, Asp911 and Met752 cannot

fittingly accommodate the large linker moiety.

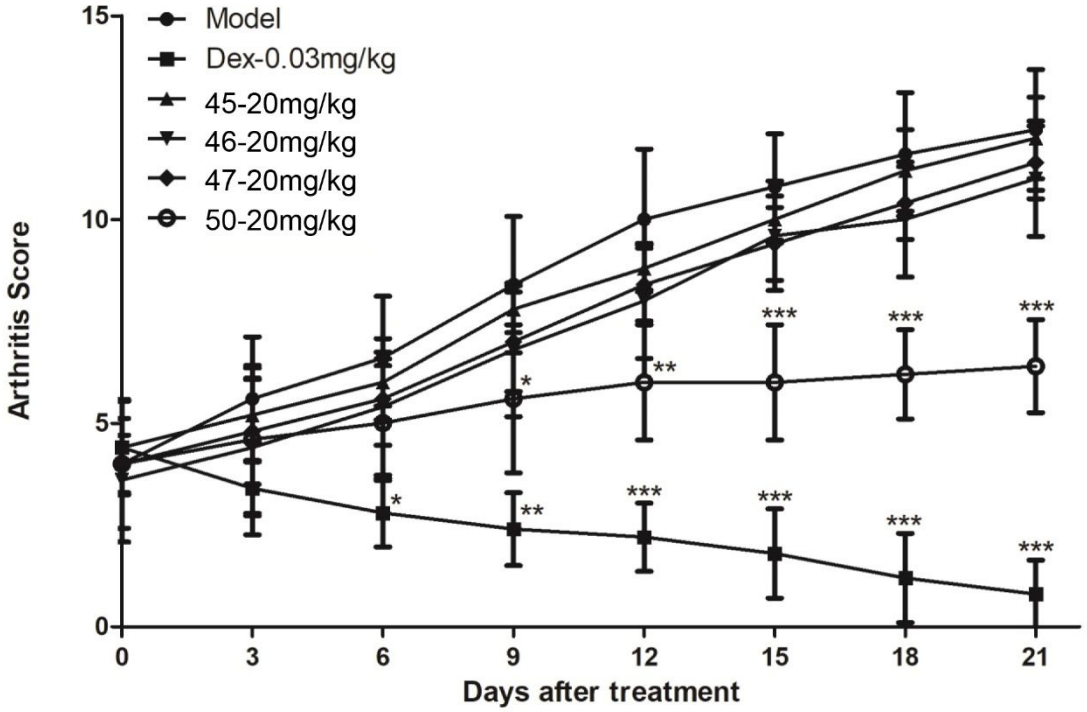

Figure S3. Pre-experiments of compound **45**, **46**, **47**, **50** and dexamethasone in collagen-induced arthritis models by oral administration once-daily.

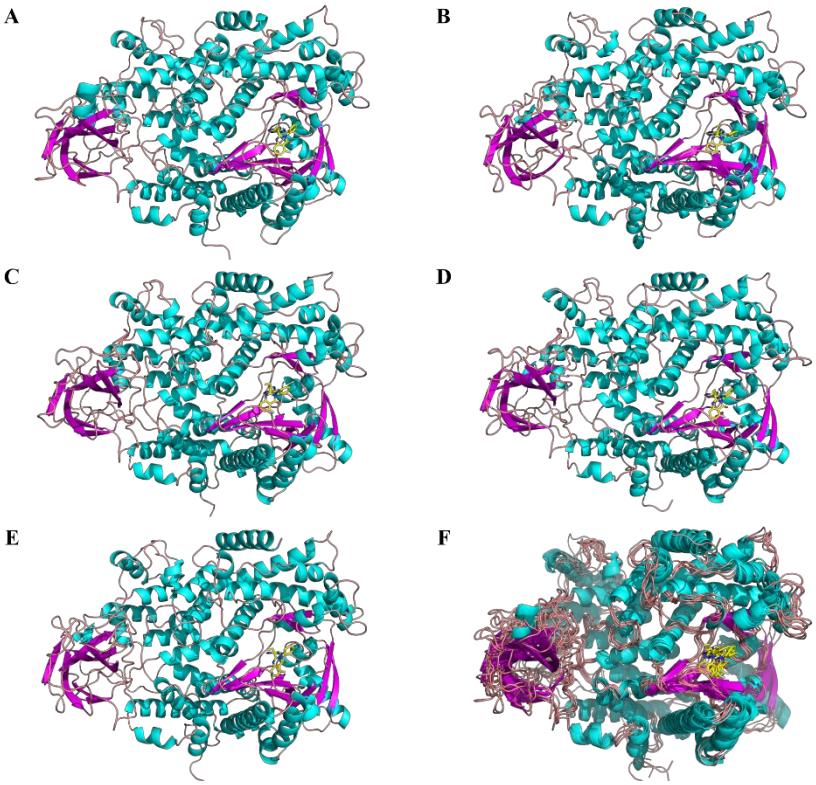

Figure S4. Snapshots of the idelalisib/ PI3Kδ complex along the dynamic simulation time for 100th, 200th, 300th, 400th and 500th ns. For clarity, the water molecules have been removed. The idelalisib is plotted using stick style, while cartoon style for PI3Kδ. (A) for 100th ns. (B) for 200th ns. (C) for 300th ns. (D) for 400th ns. (E) for 500th ns. (F) the aligned conformations.

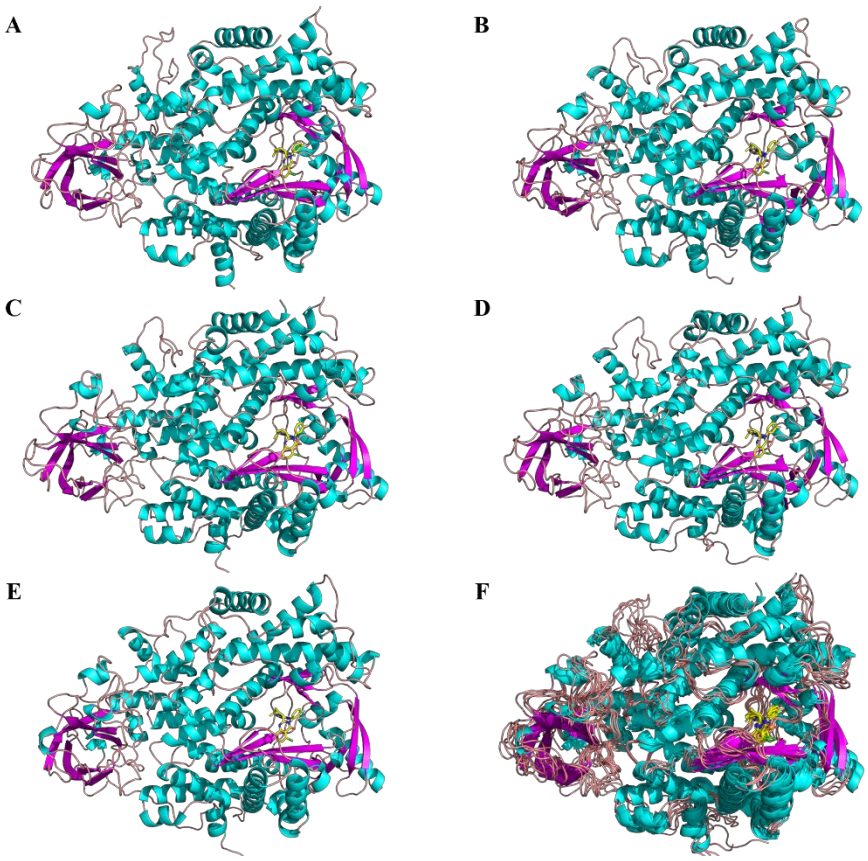

Figure S5. Snapshots of the compound **50**/ PI3Kδ complex along the dynamic simulation time at 100th, 200th, 300th, 400th and 500th ns. For clarity, the water molecules have been removed. The compound 50 is plotted using stick style, while cartoon style for PI3Kδ. (A) for 100th ns. (B) for 200th ns. (C) for 300th ns. (D) for 400th ns. (E) for 500th ns. (F) the aligned conformations.

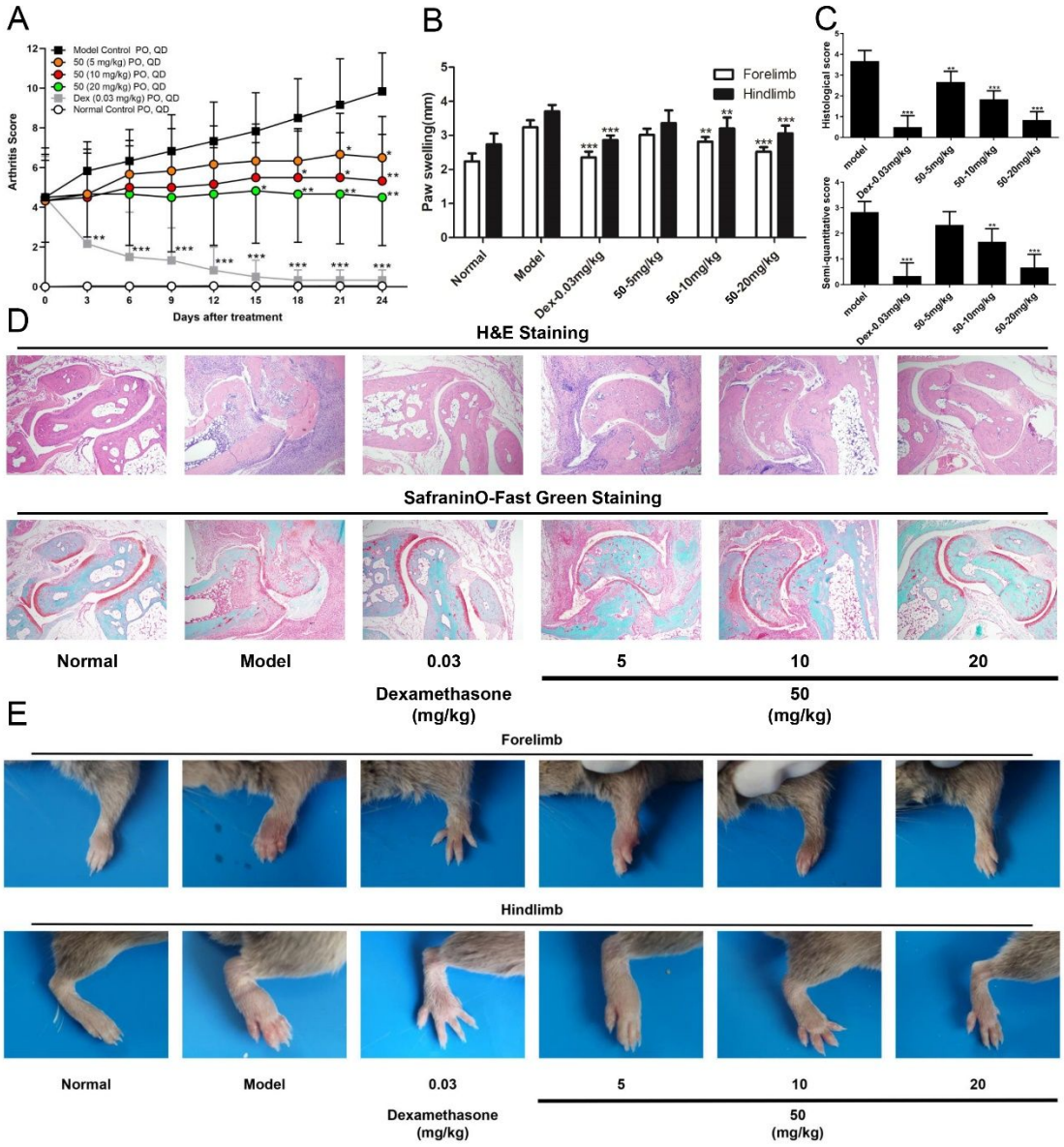

Figure S6. Therapeutic efficacy of **50** in mice established collagen-induced arthritis. (A). Clinical arthritis scores of DBA/1J mice with CIA treated with vehicle, **50** (5, 10, and 20 mg/kg), and dexamethasone (0.03 mg/kg), once daily by oral administration, for 24 days. (B) Paw swelling of forelimb and hindlimb of mice after treatment with vehicle, **50** (5, 10, and 20 mg/kg), and dexamethasone (0.03 mg/kg). Paw swelling of CIA mice was measured with a slide gauge on day 24. (C) Histopathology for ankles includes separate scores for H&E staining and safraninO-fast green staining (semi-quantitative

score). (D) Representative ankle photomicrographs from mice with the approximate mean group score from normal, model control, dexamethasone (0.03 mg/kg), **50** (5, 10, and 20 mg/kg**)**. (E) Forelimbs and hindlimbs of mice after treatment with vehicle, **50** (5, 10, and 20 mg/kg), and dexamethasone (0.03 mg/kg) on day 24. Dex = dexamethasone. The asterisk (*) denotes significance compared with vehicle control, *P < 0.05; **P < 0.01, ***P < 0.001 versus vehicle group. See Support Information for Scoring Criteria for CIA model.

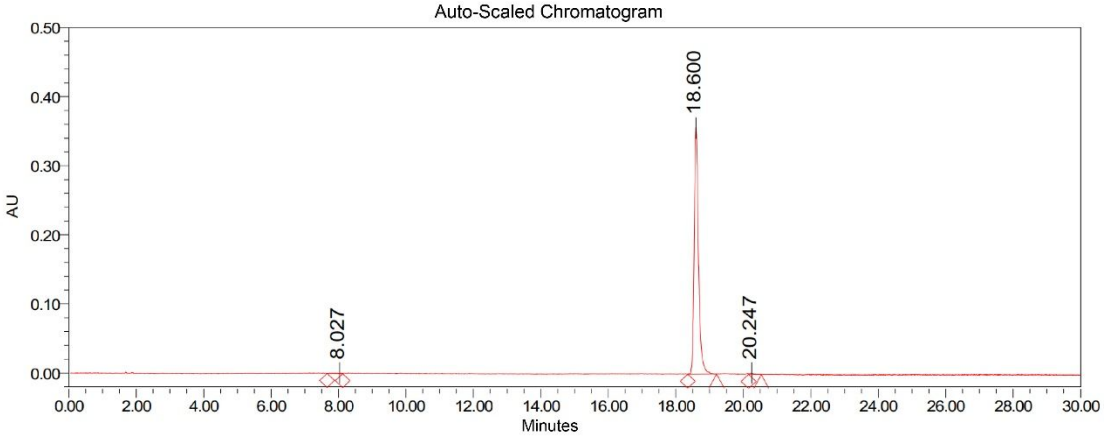

	RT	Area	Height	% Area
1	8.027	19428	961	0.60
2	18.600	3184664	356661	98.74
3	20.247	21085	2235	0.65

Figure S7. HPLC spectra of compound **50**.

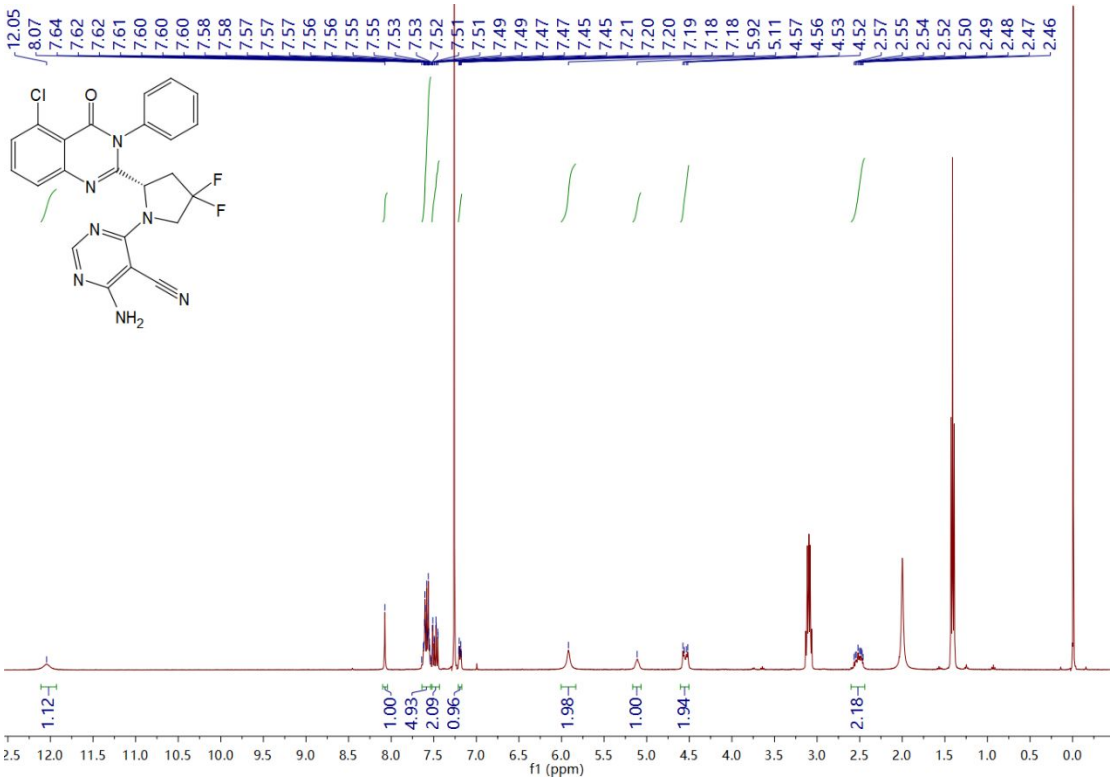

Figure S8. ^{1}H NMR spectra of compound **26**.

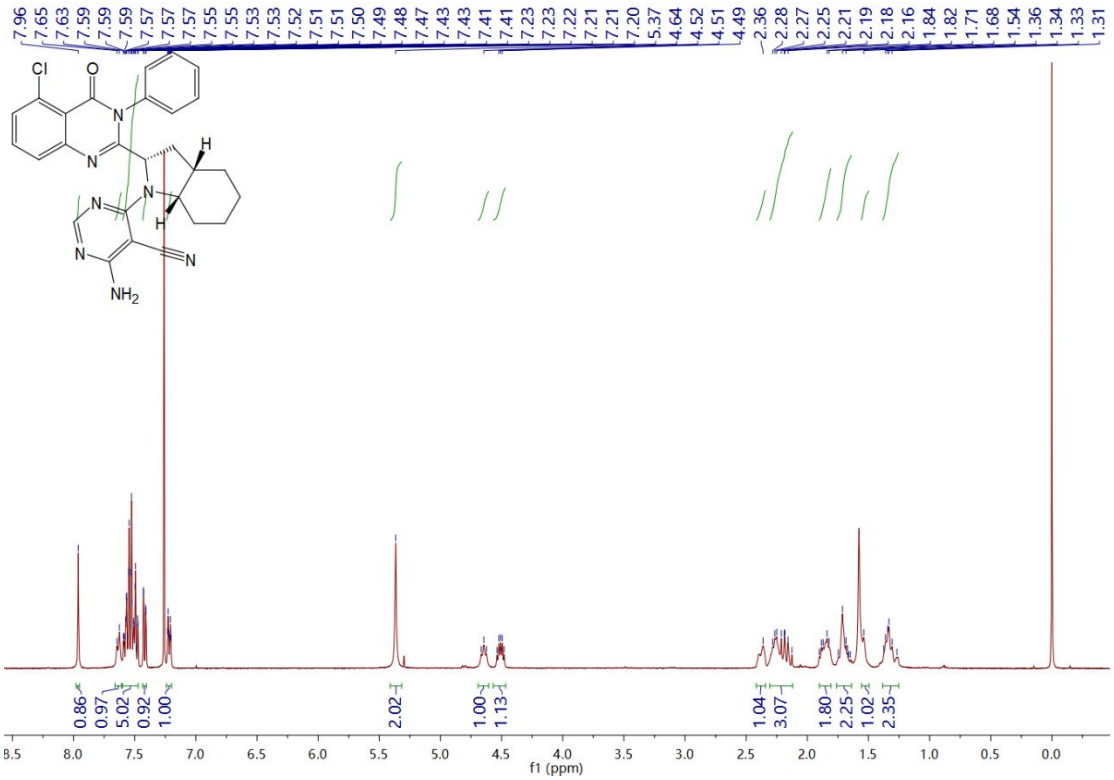

Figure S9. ^{1}H NMR spectra of compound **30**.

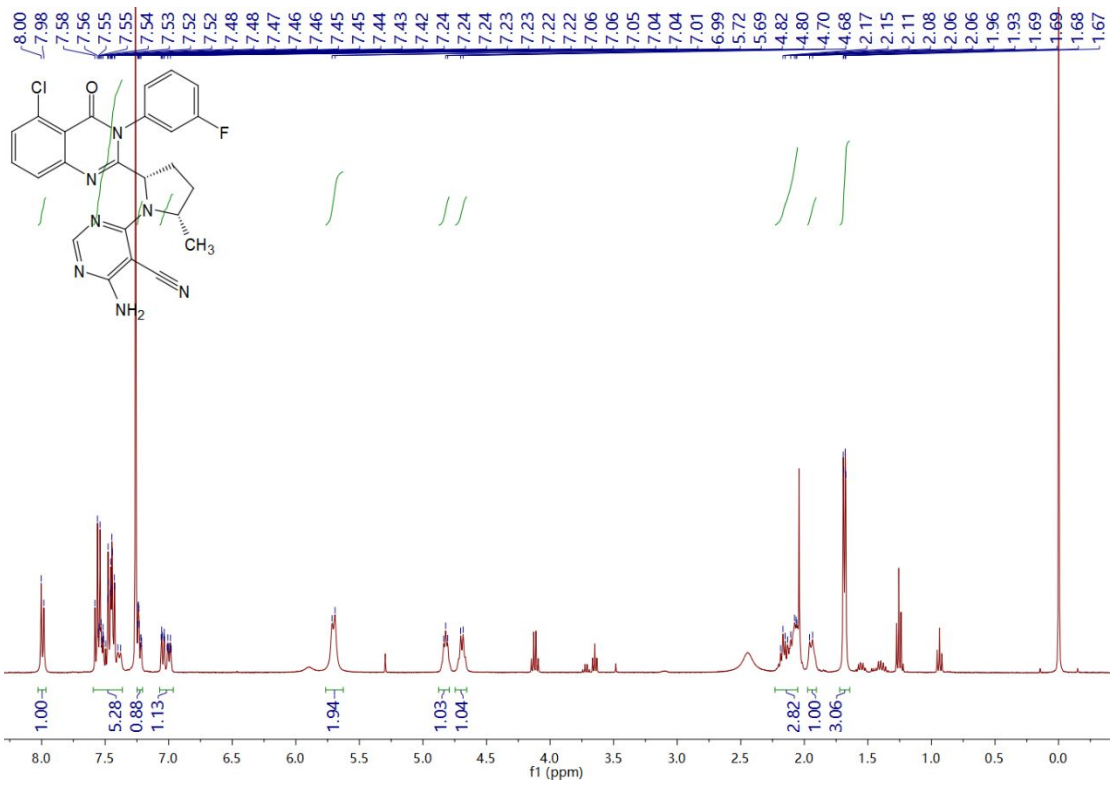

Figure S10. ^{1}H NMR spectra of compound **45**.

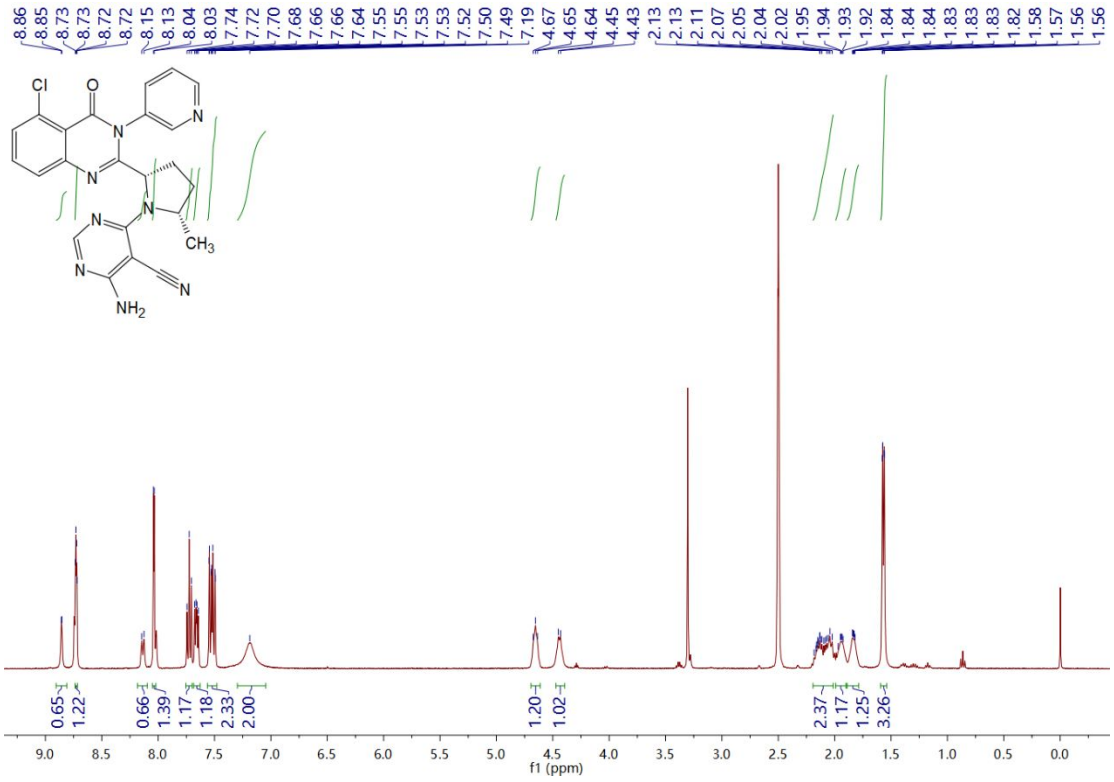

Figure S11. ^{1}H NMR spectra of compound **46**.

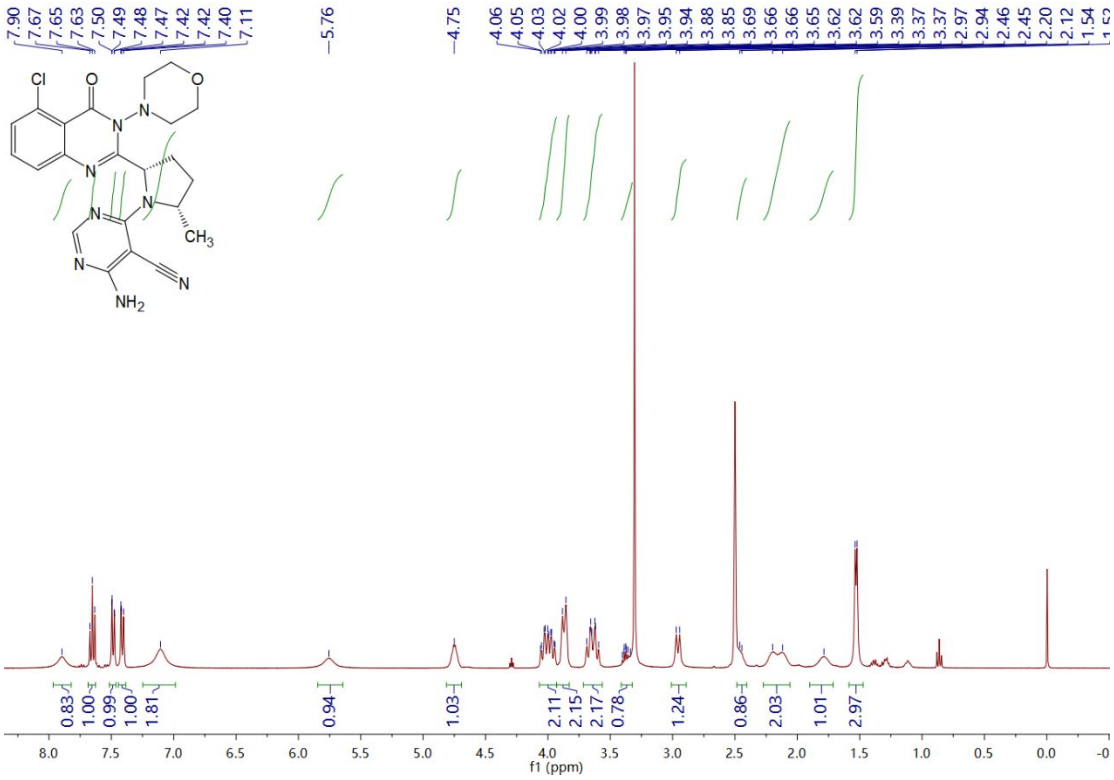

Figure S12. ^{1}H NMR spectra of compound **47**.

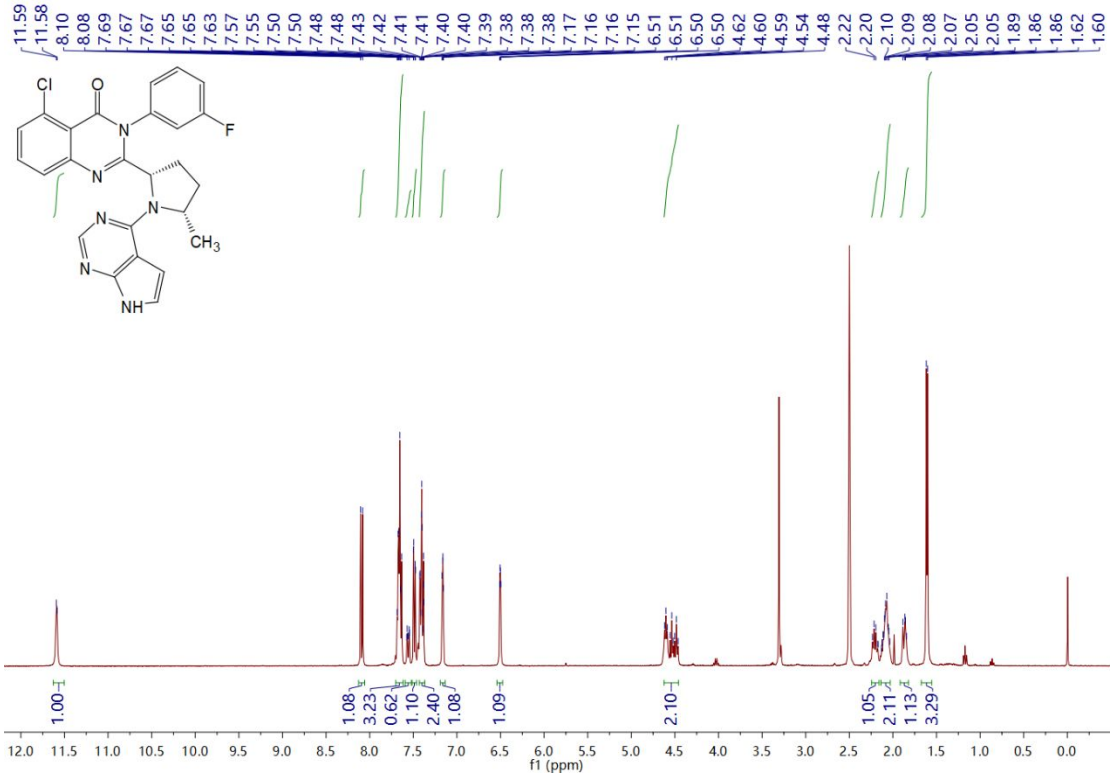

Figure S13. ^{1}H NMR spectra of compound **49**.

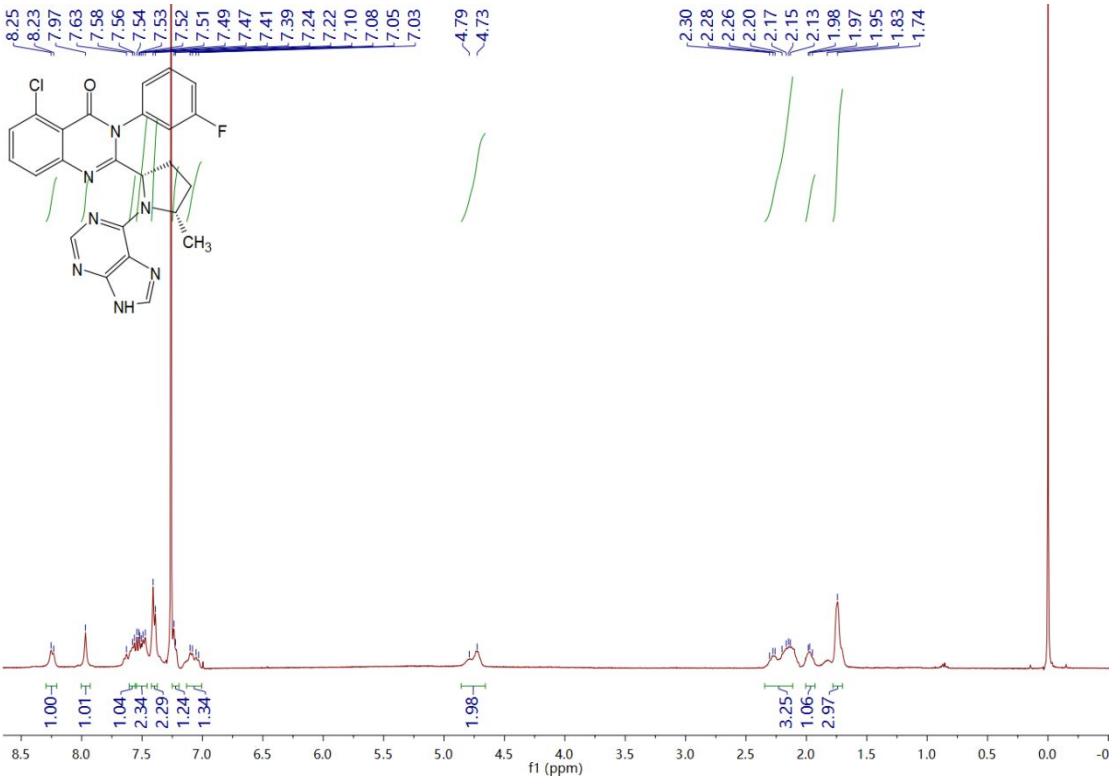

Figure S14. ^{1}H NMR spectra of compound **50**.

SMARTCyp.

Methodology of SMARTCyp.

SMARTCyp is a method for prediction of which sites in a molecule that are most liable to metabolism by Cytochrome P450. It has been shown to be applicable to metabolism by the isoforms 1A2, 2A6, 2B6, 2C8, 2C19, 2E1, and 3A4 (CYP3A4), and specific models for the isoform 2C9 (CYP2C9) and isoform 2D6 (CYP2D6) are included from version 2.1. CYP3A4, CYP2D6, and CYP2C9 are the three of the most important enzymes in drug metabolism since they are involved in the metabolism of more than half of the drugs used today.

To construct the SMARTCyp method a large number of Density Functional Theory

(DFT) calculations of fragment activation energies have been performed. The results have been compiled into rules consisting of SMARTS patterns and associated energies. SMARTCyp only uses the 2D structure of a compound, and the energy required for oxidation at each atom is computed by fragment matching towards the SMARTS patterns. If multiple patterns match the same atom the pattern with the lowest energy is used. The accessibility is approximated as the relative topological distance of an atom from the center of the molecule, and the final score is computed as Score = energy - 8*accessibility - 0.04*SASA.

The SMARTCyp 2D6 model is slightly more complex, using the basic SMARTCyp reactivity, plus the distance from an atom to the end of the molecule (Span2End), and the distance from an atom to a protonated amine nitrogen atom (N+dist). A linear correction is then applied giving a final 2D6-score = energy + 6.7*(8 - N+dist + Span2End). Cutoffs are applied so that N+dist is never larger than 8, and Span2End is never larger than 4.

The SMARTCyp 2C model is a remake of the 2D6 model, using the basic SMARTCyp reactivity, plus the distance from an atom to the end of the molecule (Span2End), and the distance from an atom to a carboxylic acid (or a bioisoster thereof) oxygen atom (COO-dist). A linear correction is then applied giving a final 2C-score = energy + 5.9*(8 - COO-dist + Span2End) - 0.04*SASA. Cutoffs are applied so that COO-dist is never larger than 8, and Span2End is never larger than 4. The detailed protocol descriptions can be provided at the website

(https://smartcyp.sund.ku.dk/interpret_smartcyp).

Explanation of Output

• The results are shown in form of a structure and a table for each molecule.

• The 3 top ranking atoms are highlighted both in the structure and table.

• The figure can be switched to showing atom numbers by hovering the mouse pointer over the figure. The atom numbers will be hidden if you move the pointer away from the figure.

• The table gives the Rank, Atom (type and number), Score, Energy, Accessibility, 2DSASA, and Similarity.

• The atoms in the tables are ranked by Score, with the lowest score resulting in the lowest rank, and thus the highest probability of being a site of metabolism.

• If the energy is 999, then there is no matching energy rule. Such sites should not be considered as possible sites of metabolism.

• While the top three sites are coloured for easier identification this does not mean there is a cutoff saying that there are always three likely sites, the score is what matters.

• The similarity is a number from 0 (low) to 1 (high). It indicates how similar the atom in the molecule is to an atom in a fragment on which the activation energies have been determined with DFT.

Molecular Docking Study. For the PI3Kδ structure-based ligand design, different crystal structures of PI3Kδ in complex with ATP, inhibitors, and apo are publicly available. However, no crystal structures of human PI3Kδ complexed with idelalisib

inhibitors are available, and only mouse PI3Kδ has been published. Therefore, the receptor protein PI3Kδ (PDB ID: 4XE0) was selected as the docking model. The protein structure was processed via PyMOL to remove the solvent molecules and the origin bound ligand. The protein structure was pretreated with the AutoDockTools, including adding hydrogen, equilibrium charge, adjustment of unreasonable atomic overlap, and so on. The molecular structures of compounds were constructed using InDraw software and saved as SDF format files. Then the molecular structures of compounds were added hydrogen at pH=7.0, adjusted pH state, generate 3D coordinates using the OpenBabel software. The molecule structures were minimized by PM3 force field by MOPAC2016. The partial charges for receptor and ligands were assigned using AutoDockTools with Gasteiger method. A grid map of 40 ×40 ×40 point with 0.375 Å grid spacing was generated using AutoGrid module based on the center of Idelalisib within 4EXO. The 100 conformations of each compound were finally generated for a 150 population size with a 2,500,000 maximum number of energy evaluation for each docking experiment using AutoDock. Subsequently, the best conformation of each docking models was remained and drawn the picture using PyMOL. The “re-docking” strategy was used to assess the docking power via the reported crystal structure for PI3Kδ complexed with idelalisib. The root mean square deviation (RMSD) between the crystal structure and the conformer with the lowest energy (-9.32 kcal/mol) from docking is 0.9 Å. To this point, we then applied molecular docking method in the construction of compound/ PI3Kδ complex structure.

Molecular Dynamics Simulation. The complex structure of idelalisib/PI3Kδ obtained from the protein data bank (PDB ID: 4XE0) and the compound **50**/PI3Kδ complex structure was constructed from the docking study. The AMBER ff19SB force field was used to create topology parameters of PI3Kδ. To correctly describe the idelalisib and compound 50 force field, the general Amber force field (GAFF) generation procedure was used. The geometry structure was optimized at B3LYP/6-31G level of theory using Gaussian 09. To obtain the partial atomic charges, the restrained electrostatic potential (RESP) protocol was employed at the HF/6-31G level of theory. The force field parameters were generated using the Antechamber module. Firstly, the complex systems were dissolved in a TIP3P water with cuboid box and the systems were neutralized using the Cl ions. To reduce the effect of unfavorable interactions produced by solvents and ion, we used three steps to minimize the complex systems for the two ligand/PI3Kδ complex systems. Following, the system was heated to 300 K and kept the pressure to 1 bar. Subsequently, the whole system underwent the 500 ns molecular dynamics for final data collection and analyses. The periodic boundary conditions were applied to avoid edge effects and a cut-off radius of 12 Å was employed for van der Waals interactions. The particle mesh Ewald (PME) algorithm also was used in calculating the long-range electrostatic interactions. The SHAKE algorithm was used to constrain the covalent bond involved with hydrogen atoms. The detail of the molecular dynamics simulation can be found in the other references.[1,2] The result was analyzed by the *CPPTRAJ*.

Binding Free Energy. To quantitatively assess the binding affinity of inhibitors with the PI3Kδ, it would be useful to calculate the corresponding binding free energies. In this work, molecular mechanics generalized Born surface area (MM/GBSA) were employed to calculate the binding free energies. For each complex system, binding energies were averaged over 1000 frames of the last 200 ns MD trajectory.

Biological Assay Methods

Enzyme assays (Non-radioactive assays). The assay was carried out by Eurofins Discovery (Cerep, France) according to the individual kinase assay protocols (non-radioactive assay). The class I PI3K isoforms were incubated in assay buffer containing 10 μM phosphatidylinositol 4,5-bisphosphate and Mg/ATP (ATP concentration was determined according to Km ATP). The reaction was initiated by the addition of the ATP solution for PI3K p110α/p85α (h) and the Mg/ATP mix for I3K (p110β/p85α) (h), PI3K (p110δ/p85α) (h), and PI3K (p120γ) (h). After incubation for 30 minutes at room temperature, the reaction was stopped by the addition of stop solution containing EDTA and biotinylated phosphatidylinositol- 3,4,5-trisphosphate. Finally, detection buffer was added, which contained europium-labelled anti-GST monoclonal antibody, GST-tagged GRP1 PH domain and streptavidin allophycocyanin. The plate was then read in time-resolved fluorescence mode and the homogeneous time-resolved fluorescence (HTRF) signal was determined according to the formula HTRF = 10000 x (Em665nm/Em620nm). The kinases activity of 10 μM **50** on 163 kinases were measured by radiometric assays or non-radioactive assays. For radiometric assay, each

kinase was incubated with 10 μM **50** in indicated reaction solutions contained [γ-^{33}P-ATP] (ATP concentration was determined according to Km ATP) and other reagents such as MOPS, EDTA, EAIYAAPFAKKK, Magnesium acetate and so on (different pH, concentrations and activities according to the specific needs of different kinases). The reaction is initiated by the addition of the Mg(n)/ATP mix. After incubation for a while (specific time as required) at room temperature, the reaction is stopped by the addition of phosphoric acid to a concentration of 0.5%. 10 μL of the stopped reaction is spotted onto a P30 filtermat and washed four times for 4 minutes in 0.425% phosphoric acid and once in methanol prior to drying and scintillation counting. For non-radioactive assay, each kinase was incubated with 10 μM **50** in assay buffer containing Mg/ATP (ATP concentration was determined according to Km ATP) and other regents such as phosphatidylinositol 4,5-bisphosphate, phosphatidylinositol, phosphatidylserine, GST-cMyc-p53, and so on (different compositions and concentrations according to the specific needs of different kinases). The reaction is initiated by the addition of the ATP solution or the Mg/ATP mix. After a period of incubation (different kinases require different time) at room temperature, the reaction is stopped by the addition of stop solution containing EDTA or other regents such as biotinylated phosphatidylinositol- 3,4,5-trisphosphate (different compositions and concentrations according to the specific needs of different kinases). Finally, detection buffer is added, which contains europium-labelled anti-GST monoclonal antibody or other regents such as GST-tagged GRP1 PH domain and streptavidin allophycocyanin

(different compositions and concentrations according to the specific needs of different kinases). The plate is then read in timeresolved fluorescence mode and the homogeneous time-resolved fluorescence (HTRF) signal is determined according to the formula HTRF = 10000 x (Em665nm/Em620nm). The in vitro kinase enzymatic inhibition assays were carried out by the Kinase Profiling Services provided by Eurofins (France). The detailed protocol descriptions can be provided at the website: https://www.eurofinsdiscoveryservices.com

Class I PI3K Isoform-Selective Cellular Assays

Class I PI3K isoform-selective cellular assays were performed under analogous conditions as reported (Winkler, D. G. et al. *Chem. Biol.* **2013**, *20*, 1364-1374).[3] SKOV-3, 786-O, RAW264.7 and RAJI cell lines were purchased from ATCC (Manassas, VA). Cell culture was performed under aseptic conditions.

PI3Kα Assay Design

SKOV-3 cells were seeded into 96-well cell culture-grade plates at a density of 200,000 cells/200 μL/well of RPMI-1640 with 10% FBS. Cells were incubated overnight at 5% CO_2 and 37°C. Compound **50** was added to the cells, resulting in a final DMSO concentration of 0.5%, and incubated for 30 minutes at 5% CO_2 and 37°C. Media was then aspirated and 50 μL/well of ice-cold lysis buffer was added. Plates were incubated on ice for 5 minutes and then centrifuged at 3000 rpm at 4 °C for 5 minutes.

PI3Kβ Assay Design

786-O cells were seeded into 96-well cell culture-grade plates at a density of 200,000

cells/200 µL/well of DMEM with 10% FBS. Cells were incubated overnight at 5% CO_2 and 37 °C. Compound **50** was added to the cells, resulting in a final DMSO concentration of 0.5%, and incubated for 30 minutes at 5% CO_2 and 37°C. Media was then aspirated and 50 µL/well of ice-cold lysis buffer was added. Plates were incubated on ice for 5 minutes and then centrifuged at 3000 rpm at 4°C for 5 minutes.

PI3Kγ Assay Design

RAW264.7 cells were seeded into 96-well cell culture-grade plates at a density of 200,000 cells/200µL/well of RPMI-1640 with no FBS added. Cells were incubated overnight at 5% CO_2 and 37°C. Following 18 hours of serum-starvation, compound **50** was added to the cells, resulting in a final DMSO concentration of 0.5%, and incubated for 30 minutes at 5% CO_2 and 37°C. Cells were then stimulated with 25 nM C5a (RnD Systems) for 3 minutes. Media was aspirated and 50 µL/well of ice-cold lysis buffer was added. Plates were incubated on ice for 5 minutes and then centrifuged at 3000 rpm at 4°C for 5 minutes.

PI3Kδ Assay Design

RAJI cells were seeded into 96-well cell culture-grade plates at a density of 200,000 cells/200 µL/well of RPMI-1640 with no FBS added. Cells were incubated overnight at 5% CO_2 and 37°C. Following 18 to 24 hours of serum-starvation, Compound **50** was added to the cells, resulting in a final DMSO concentration of 0.5%, and incubated for 30 minutes at 5% CO_2 and 37°C. Cells were then stimulated with 10 µg/mL anti-human IgM (Jackson ImmunoResearch) for 30 minutes in the presence of **50**. Media was

aspirated and 50 µL/well of ice-cold lysis buffer was added. Plates were incubated on ice for 5 minutes and then centrifuged at 3000 rpm at 4°C for 5 minutes.

ELISA Data Analysis

Lysates from the 4 isoform-selective assays were added to the pAKT ELISA plate without dilution. The ELISA was completed following the manufacturer's protocol. Absorbance at 450 nm was read on a SpectraMax plate reader. For SKOV-3 and 786-O cell assays, there is no stimulation thus the negative control is cells treated only with DMSO. Inhibition isotherms of AKT phosphorylation were generated by plotting the % inhibition against the inhibitor concentration, and the IC_{50} values were determined by fitting to a 4 parameter logistics equation utilizing non-linear least squared regression analysis via the program KaleidaGraph.

Basophil Activation Assay in HWB.

Basophil activation was measured in human whole blood using the Flow2 CAST kit (Buhlmann Laboratories, Switzerland) following the protocol provided by the manufacturer with minor modifications. Human whole blood was collected into K2-EDTA venipuncture tubes. Whole blood samples were incubated with either DMSO (0.3% final) or a serial dilution of **50** in DMSO for 60 min at 37 °C. To activate basophils using the anti-FceRI mAb; 50 µL of whole blood was mixed with 130 µL of stimulation buffer and 10 µL of anti-FceRI. Stimulation buffer alone was used as a negative control. The cells were stained with anti-CD63-FITC and anti-CCR3 (CD193)-PE antibodies for 25 min at 37°C. 2 mL lysis solution was added to lyse

erythrocytes to fix blood cells. After a 10 min incubation at room temperature, cells were pelleted and resuspended in wash buffer and analyzed by flow cytometry. Degranulation was detected via CD63 surface expression on CCR3 positive cells. The percent CD63 positive cells within the gated basophil population was determined in different treatment groups and normalized to the vehicle control (0.3% DMSO). Data were plotted using the Prism software, and IC_{50} values were determined. Data were analyzed via one-way analysis of variance (ANOVA), followed by Dunnett's test.

B Cell Activation Assay in HWB.

Whole blood was pretreated with **50** for 60 min. The blood was stimulated with anti-IgM (Jackson ImmunoResearch) at 37°C overnight. After red blood cell (RBC) depletion, cells were harvested and stained with APC-labeled anti-CD19 antibody (BD Biosciences) and fluorescein isothiocyanate (FITC)-labeled anti-CD69 antibody (BD Biosciences) for flow cytometry analysis. Activated B-cells were gated based on B220 and CD86 expressions. The ratio of $CD19^{+}CD69^{+}$ positive cells in compound-treated blood as compared to the untreated control was used to determine the percent inhibition by compound treatment. Data were plotted using the Prism software, and IC_{50} values were determined. Data were analyzed via one-way ANOVA, followed by Dunnett's test.

Primary Human T-cell Proliferation Assays

Human peripheral blood $CD3^{+}$ T-cells were purchased from Allcells (Emeryville, CA). Pre-diluted compound in DMSO or DMSO alone (control) were incubatedwith cells

(100,000 cells in RPMI-1640 media supplemented with 10% fetal calf serum, penicillin, streptomycin and 50 μM β-mercaptoethanol) for 1 hour at 37°C (final DMSO 0.1%). For stimulation of T-cell proliferation, a cocktail consisting of ConA (Sigma Aldrich) was added yielding a final concentration of 5μg/mL. Cells were incubated at 37°C with 5% CO2 for 72 hours to get optimal signal to noise for each assay. Cell number was measured using the CellTiter-Glo Luminescent Cell Viability Assay reagent (Promega).

Microsome Stability Assay. Human liver microsomes and reduced nicotinamide adenine dinucleotide phosphate (NADPH, solution A 2.5mL and solution B 0.5mL) were both supplied by Wuhan PrimeTox Bio-pharma Technology Co., Ltd. Metabolic stability in vitro was determined using pooled hepatic microsomal fractions at a final test compound concentration of 1 μM. In general, incubation mixtures consisted of 0.1 M potassium phosphate buffer at pH 7.4, NADPH regenerating system (containing 1 mM NADP, 5 mM D-Glucose-6-phosphate, 1 U/mL glucose 6-phosphatedehydrogenase, and 3.3 mM $MgCl_2$) with a final volume of 100 μL. The stock solution of the test compound and SAHA (internal standard, IS) were prepared with methanol first and then diluted to designated concentration. The solution of the test compound (0.5μL, 200μM/L) was added into the incubation mixtures in an ice bath, then the incubation system was put into 37°C water bath for pre-incubation. The solution of human liver microsomes (2.5 μL, 20 mg/mL) was added into the incubation mixtures after 5 minutes. The incubation was typically terminated by adding 200 μL cold acetonitrile containing IS (10ng/mL) at various time points (0, 5, 15, 30, 45, and

60min). The terminated incubation mixtures were centrifuged at 13000 rpm for 15 min, and then supernatant was injected for analysis.

Pharmacokinetic Study. Sprague-Dawley rats were supplied by Chengdu Dossy Experimental Animals Co., Ltd. A 1 mg/mL dosing solution of **50** was prepared by dissolving in physiological saline containing 1% DMSO, 1% Tween 80 for po or iv administration. Six SD rats, weighing 200−250 g each, were obtained from Chengdu Dossy Experimental Animals Co., Ltd. The tested compound was separately administered intravenously (5 mg/kg dose) or orally (5 mg/kg) to a group of six rats per time. At time points 0 (prior to dosing), 5 min, 15 min, 30 min, 45 min, 1 h, 2 h, 4 h, 6 h, 8 h, 10 h, 12 h, and 24 h after dosing, a blood sample was collected from each animal via cardiac puncture and stored in refrigerator (−20℃). Plasma was separated from the blood by centrifugation (4000 g for 15 min at 4℃) and stored in a freezer at −80℃. All samples were analyzed for the tested compound by LC−MS/MS (Waters Acquity UPLC system; Waters Quattro Premier XE). Data were acquired via monitoring of multiple reactions. Plasma concentration data were analyzed by a standard noncompartmental method.

Collagen-Induced Arthritis (CIA) Model.

DBA1/J male mice (6-8 weeks old) were obtained from Beijing HFK Bioscience Co., Ltd, and maintained in specific pathogen free air at a temperature of 22 ± 2°C on a 12-h light/dark cycle with food and water ad libitum and relative humidity of 50%. Standard laboratory chow and water ad libitum were ensured. The animal protocol was

approved by the Animal Care and Use Committee of Sichuan University in China (IACUC number: 20100318). One day before the start of the experiment, CII solution (2 mg/ml) was prepared with 0.05 M acetic acid and stored at 4°C. Just before the immunization, equal volumes of IFA and CII were mixed by a homogenizer in a precooled glass bottle in an ice water bath. Arthritis was induced by subcutaneous injection with a 1:1 emulsion of bovine type II collagen (Chondrex) and Freund's complete adjuvant (Sigma-Aldrich) at the base of the tail. On day 21, Mice were suffered a booster injection with a 1:1 emulsion of bovine type II collagen in Freund's incomplete adjuvant (Sigma-Aldrich) at the tail, but at a different location from the site of first injection. Thereafter, all mice were monitored daily for signs of arthritis: redness and swelling of a fore or hind paw. On the day treatment was initiated, mice were randomly divided into several groups with each containing the same number of animals, and then treated with vehicle (the group of Model), 0.03 mg/kg Dexamethasone, 20 mg/kg CAL-101, 5, 10, and 20 mg/kg compound **50**, respectively (pharmaceutical solution formulations: 2% dimethyl sulfoxide, 30% polyethylene glycol 400, 0.5% polysorbate 80, and 5% sodium carboxymethyl cellulose solution). The treatment continued for 24 or 27 days, during which the arthritis index was measured every three days. For the development of CIA and inflammation of the four paws was graded from 0 to 4: grade 0, paws with no swelling and focal redness; grade 1, paws with swelling of finger joints; grade 2, paws with mild swelling of ankle or wrist joints; grade 3, paws with severe inflammation of the entire paw; and grade 4,

paws with deformities or ankyloses. Each paw was graded and the four scores were totaled so that the possible maximum score per mouse was 16.[4,5]

Histological Examination.

DBA1/J mice were sacrificed on day 24 after treatment and ankle joints were removed and fixed with 4% paraformaldehyde for more than 48 h. The joints were decalcified in EDTA buffer for 21 days and then embedded in paraffin blocks. Joint sections were stained with H&E or safranin O-fast green. The histological changes were examined under microscope. All sections were evaluated histologically by two independent observers. For H&E, the gradation of arthritis was scored from 0 to 4 according to the intensity of lining layer hyperplasia, mononuclear cell infiltration, and pannus formation, as described previously[6]. 0, normal ankle joint; 1, normal synovium with occasional mononuclear cells; 2, definite arthritis, a few layers of flat to rounded synovial lining cells and scattered mononuclear cells; 3, clear hyperplasia of the synovium with three or more layers of loosely arranged lining cells and dense infiltration with mononuclear cells; 4, severe synovitis with pannus and erosions of articular cartilage and subchondral bone. Safranin O staining was scored with a semiquantitative scoring system (0–3), where 0 represents no loss of proteoglycans and 3 indicates complete loss of staining for proteoglycans.[7]

Reference:

(1) Wang, P.; Mao, L.; Shi, M.; Fu, Y.; Jiang, X.; Feng, W.; He, Y.; Xu, D.; Yuan, L. The Cytochrome c–Cyclo[6]Aramide Complex as a Supramolecular Catalyst

in Methanol. *New J. Chem.* **2018**, *42* (5), 3857–3866.

(2) Xiaoqin; Wang; Zhi-Min; Li; Qingyue; Mingsong; Shi; Lingling; Bao; Dingguo. Purification and Biochemical Characterization of FrsA Protein from Vibrio Vulnificus as an Esterase. *PLoS One* **2019**, *14* (4): e0215084.

(3) Winkler, D. G.; Faia, K. L.; Dinitto, J. P.; Ali, J. A.; White, K. F.; Brophy, E. E.; Pink, M. M.; Proctor, J. L.; Lussier, J.; Martin, C. M.; Hoyt, J. G.; Tillotson, B.; Murphy, E. L.; Lim, A. R.; Thomas, B. D.; MacDougall, J. R.; Ren, P.; Liu, Y.; Li, L. S.; Jessen, K. A.; Fritz, C. C.; Dunbar, J. L.; Porter, J. R.; Rommel, C.; Palombella, V. J.; Changelian, P. S.; Kutok, J. L. PI3K-δ and PI3K-γ Inhibition by IPI-145 Abrogates Immune Responses and Suppresses Activity in Autoimmune and Inflammatory Disease Models. *Chem. Biol.* **2013**, *20* (11), 1364–1374.

(4) Hegen, M.; Keith, J. C.; Collins, M.; Nickerson-Nutter, C. L. Utility of Animal Models for Identification of Potential Therapeutics for Rheumatoid Arthritis. *Ann. Rheum. Dis.* **2008**, *67* (11), 1505–1515.

(5) Alonzi, T.; Fattori, E.; Lazzaro, D.; Costa, P.; Probert, L.; Kollias, G.; De Benedetti, F.; Poli, V.; Ciliberto, G. Interleukin 6 Is Required for the Development of Collagen-Induced Arthritis. *J. Exp. Med.* **1998**, *187* (4), 461–468.

(6) Brackertz, D.; Mitchell, G. F.; Mackay, I. R. Antigen-Induced Arthritis in Mice. I. Induction of Arthritis in Various Strains of Mice. *Arthritis Rheum.*

1977, *20* (3), 841–850.

(7) Dudler, J.; Renggli-Zulliger, N.; Busso, N.; Lotz, M.; So, A. Effect of Interleukin 17 on Proteoglycan Degradation in Murine Knee Joints. *Ann. Rheum. Dis.* **2000**, *59* (7), 529–532.